Nano Research

Open Access

Research Article

Interfacial integration and molecular orientation control enable large-scale production of high-performance spider silk-inspired multifilaments

Wenhao Cheng[1,2], Wei Wang[3], Lingpeng Meng[3], Yawei Liu[4] ✉, Sikang Wan[5] ✉, Kai Liu[1,3,5], Juanjuan Su[6] ✉, and Hongjie Zhang[1,2,5]

[1] *Changchun Institute of Applied Chemistry, Chinese Academy of Sciences, Changchun 130022, China*
[2] *School of Applied Chemistry and Engineering, University of Science and Technology of China, Hefei 230026, China*
[3] *Xiangfu Laboratory, Jiaxing 314102, China*
[4] *State Key Laboratory of Synthetic Biology and School of Synthetic Biology and Biomanufacturing, Tianjin University, Tianjin 300072, China*
[5] *Engineering Research Center of Advanced Rare Earth Materials (Ministry of Education), Department of Chemistry, Tsinghua University, Beijing 100084, China*
[6] *Center of Materials Science and Optoelectronics Engineering, College of Materials Science and Optoelectronic Technology, University of Chinese Academy of Sciences, Beijing 100049, China*

Cite this article: *Nano Research*, **2026**, *19*, 94908927. https://doi.org/10.26599/NR.2026.94908927

ABSTRACT: Spider silk-inspired fibers have attracted great attentions for their potential to combine high strength and high toughness. However, their production remains predominantly confined to the laboratory stage, hindered by formation continuity and performance stability upon scale-up. Herein, large-scale continuous production of spider silk-inspired multifilaments with high strength and toughness was realized using custom-designed spinning system. Coagulation bath was modulated to control solvent exchange process during spinning, thereby facilitating interfacial integration and improved molecular orientation. In addition, post-stretching process was optimized to further promote molecular orientation and crystal formation. After systematic process optimization, the large-scale continuous production of spider silk-inspired multifilaments with a robust and stable tensile strength of 234.54 ± 7.37 MPa and a toughness of 184.68 ± 20.91 MJ/m³ was achieved. This custom-designed spinning system enabled continuous spinning for more than 8 h, yielding multifilaments exceeding 18 km in length. This work provides a feasible strategy for the large-scale continuous production of spider silk-inspired multifilaments, bridging the gap toward practical applications.

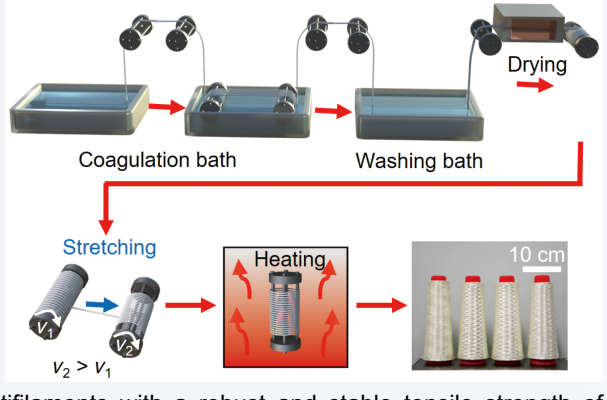

KEYWORDS: large-scale spinning, multifilament, spider silk-inspired fiber, assembly

1 Introduction

Spider silk exhibits a combination of remarkable strength and toughness, surpassing the mechanical performance of most artificial fibers [1–4]. Unfortunately, the large-scale collection of nature spider silk is difficult due to low yield of spidroins and the aggressiveness of spider [5–7]. The high performance of spider silk originates from its microstructure, in which highly ordered β-sheet nanocrystals are embedded in soft amorphous domains [8–10]. Inspired by this microstructure, recombinant proteins integrating high β-sheet structure content and amorphous domains were widely engineered for silk spinning [8, 11]. Through the incorporation of β-sheet structures, the spider silk-inspired protein fibers achieved superior mechanical performance [12–14]. However, owing to the limited yield of recombinant proteins and the difficulty in controlling the protein assembly process, the large-scale production of spider silk-inspired protein fibers with robust and stable mechanical performance still remains challenge [15].

Received: May 9, 2026; **Revised:** June 5, 2026
Accepted: June 8, 2026

✉Address correspondence to Yawei Liu, ywliu_0722@tju.edu.cn; Sikang Wan, skwan@tsinghua.edu.cn; Juanjuan Su, sujuanjuan@ucas.ac.cn

Natural or synthetic polymers with molecular structure similar to spidroins (such as polyurethane (PU) [16, 17], polyvinyl alcohol (PVA)-polyacrylic acid (PAA) [18], and regenerated silk fibroin [19, 20]) can serve as a temporary alternative for producing spider silk-inspired fibers with high strength and toughness. Particularly, PU consists of alternating soft and hard segments, resembling the structure of spidroins, which is often used to prepare spider silk-inspired materials. For example, PU-based pseudoprotein fibers demonstrate exceptional toughness and tensile strength by mimicking the microstructure of spider silk [16]. In contrast to the recombinant spidroins or regenerated silk fibroins, which require expensive fermentation and purification or complex degumming process, PU is commonly derived from petrochemicals. Consequently, PU is commercially available and produced globally on a ten-million-ton scale at low cost, making it particularly well-suit for scalable production and applications. However, current efforts in spider silk-inspired fibers have primarily focused on controlling the assembly process to produce high-performance fibers at the laboratory scale, with less attention to large-scale production, which greatly restricts their practical applications [21, 22]. Compared to the relatively simple control conditions at the laboratory scale, which mainly require regulation of intrinsic microphase structure, scalable production of multifilament places stringent demands on the yield and uniformity of the entire spinning process. Therefore, it is imperative to develop a mass production system and processes for large-scale producing spider silk-inspired multifilaments with robust and stable mechanical performance.

In this work, the continuous large-scale production of spider silk-inspired multifilaments with high strength and toughness was realized using custom-designed spinning system (Fig. 1(a)). Polyurethane, with an alternating structure of soft and hard segments similar to the molecular structure of spidroins, was used to prepare spider silk-inspired multifilaments [17, 23, 24]. The molecular orientation of multifilaments was improved by regulating molecular assembly in the coagulation bath, resulting in enhanced mechanical properties. The slow filament formation rate resulted in an incompletely solidified surface, which promoted the formation of better-fused and oriented multifilaments, resulting in improved strength and toughness (Fig. 1(b)). In addition, post-treatment was applied to further enhanced the tensile strength of multifilaments by promoting crystals formation and molecular alignment (Fig. 1(c)). Afterwards, complete solvent exchange in the coagulation bath and washing process was further designed and tuned to optimized the whole spinning process. As a result, the continuous production of multifilaments with a tensile strength of 234.54 ± 7.37 MPa and a toughness of 184.68 ± 20.91 MJ/m^3 was realized for at least 8 h, yielding multifilaments up to 18 km in length. In summary, this work achieved large-scale continuous production of spider silk-inspired multifilaments with robust and stable mechanical performance using custom-designed spinning system, facilitating the transition of laboratory research into practical production. The spider silk-inspired multifilaments combine high strength and toughness, offering great potential for diverse applications such as anti-thrombotic stockings, impact-resistant fabrics, and ballistic vests.

2 Experimental

2.1 Coagulation solvent modulation

In general, polyurethane was dissolved in dimethyl sulfoxide (DMSO) at a concentration of 15 wt.%, unless otherwise noted. For preparing as-spun multifilaments, the polyurethane solution was extruded from the multi-channel microfluidic device into the coagulation bath using a syringe pump (LSP01-3A, Longer). The solution extrusion rate was set as 8 μL/min for each channel. The coagulation solvents were set as methanol, ethanol, and isopropanol. The filament count of multifilaments was regulated by controlling the number of channels in a multi-channel microfluidic device. The as-spun multifilaments were automatically collected on a rotating collector driven by a motor (86HBP115AL4S, Beijing Haijiejiachuang Technology Co., Ltd., China) and dried in the air for 2 h. The collection speed was set as 1 m/min. Afterwards, the mechanical performance of the multifilaments coagulated with different solvents was compared.

2.2 Characterization

The small-angle X-ray scattering (SAXS) test of multifilament was performed using synchrotron radiation at BL19U2 station of Shanghai Synchrotron Radiation Facility (SSRF). The X-ray wavelength was 0.103 nm. The sample-to-detector distance was 2718.6 mm. The 10-filament multifilament was mounted on a hollow specimen holder with double-sided adhesive tapes. The wide-angle X-ray scattering (WAXS) measurements of multifilament were performed using synchrotron radiation at BL16B1 station of SSRF. The X-ray wavelength was 0.124 nm. The sample-to-detector distance was 293.2 mm. The 10-filament multifilament was mounted on a hollow specimen holder with double-sided adhesive tapes. Polarized Raman spectra of the samples were recorded using a Renishaw inVia Raman spectrometer (England). All spectra were normalized to the intensity of the 1617.7 cm^{-1} peaks. The bands of free C=O at 1731.5 cm^{-1} were used for calculating peak intensity ratio ($I_{0°}/I_{90°}$)[8].

3 Results and discussion

3.1 Fabrication of multifilaments with superior fusion and mechanical properties via coagulation bath regulation

The spider silk-inspired multifilament was fabricated through wet-spinning technology. The detailed as-spinning process of spider silk-inspired multifilament is shown in Fig. 2(a). Polyurethane is a block polymer with an alternating structure of soft and hard segments, which is similar to the soft amorphous domains and β-sheet nanocrystals of spidroins, and was used to prepared spider silk-inspired multifilaments. Polyurethane polymer spinning solution was extruded from spinneret into coagulation bath, forming the as-spun filaments through solvent exchange process. To explore the multifilaments spinning process, three-dimensional (3D) printing multi-channel microfluidic devices with different channel numbers of 3, 6, and 10 were designed to prepare spider silk-inspired multifilaments. Since the solvent exchange process holds significant impact on filament formation and properties, different alcohol solutions (including methanol, ethanol, and isopropanol) were applied as coagulation bath to control fiber solidification and multifilament fusion. The surface and cross-section morphologies of multifilaments formed in different coagulation baths were observed using scanning electron microscopy (SEM) (Fig. 2(b) and Figs. S1–S4 in the Electronic Supplementary Material (ESM)). The isopropanol-coagulated multifilaments consisting of 3, 6, or 10 filaments showed smoother surfaces than corresponding

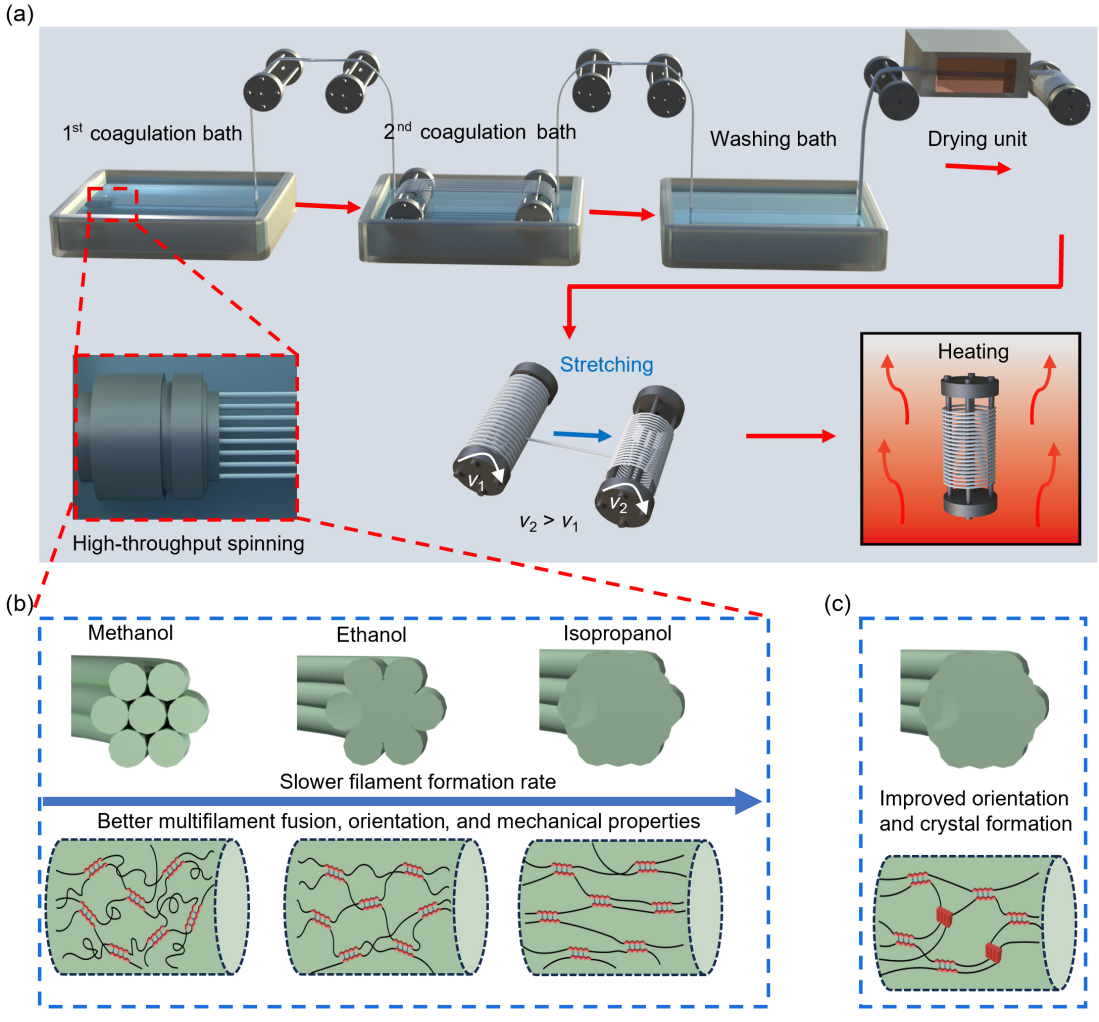

Figure 1 Schematic diagram showing continuous large-scale production of spider silk-inspired multifilaments. (a) The custom-designed spinning system for continuous large-scale production of spider silk-inspired multifilaments. (b) The schematic mechanism illustrating how coagulation solvents modulate the structure and performance of multifilaments. Coagulation bath solvents affected the filament formation rate, which influenced orientation degree and filament fusion, thereby ultimately modulating the mechanical properties of multifilaments. (c) The schematic mechanism illustrating the structure of the post-stretched multifilaments. Post-stretching and heating promoted molecular chain rearrangement, leading to improved orientation and crystal formation.

multifilaments solidified in methanol or ethanol coagulation baths. More importantly, cross-section images confirmed that the isopropanol-coagulated multifilaments exhibited the best fusion, highlighting the significant role of coagulation bath on preparing superior fused multifilaments. The better fusion in isopropanol-coagulated multifilaments was also supported by tensile test (Fig. S5 in the ESM). The stress–strain curves of 3-filament and 6-filament multifilaments formed in methanol coagulation bath showed staircase-like dopes due to inhomogeneous fracture. In contrast, multifilaments formed in ethanol and isopropanol exhibited synchronous fracture bahavior. In addition, as coagulation bath changed from methanol to ethanol and then to isopropanol, the toughness, strain, tensile strength, and ultimate tensile force of all multifilaments were improved significantly (Figs. 2(c)–2(e), and Fig. S6 and Table S1 in the ESM). The tensile strengths were 45.46 ± 2.61, 55.57 ± 5.04, and 82.80 ± 7.83 MPa for as-spun 10-filament multifilaments formed in methanol, ethanol, and isopropanol coagulation baths, respectively. Their corresponding toughness values were 138.16 ± 12.76, 222.36 ± 28.25, and 444.39 ± 82.65 MJ/m^3, respectively. Notably, the mechanical performance of the multifilaments was mainly determined by the coagulation bath. The number of orifices influenced the overall diameter owing to the fusion of the filaments, but not significantly attenuated their tensile strength and toughness. Therefore, isopropanol was selected as the coagulation bath for the large-scale production of spider silk-inspired multifilament.

To investigate how the coagulation bath influenced the mechanical performance of the multifilaments, the molecular orientation degrees and crystalline structures of different multifilaments were examined. The molecular orientation degrees of multifilaments formed in different coagulation baths were investigated using crossed polarized optical microscopy (POM). As shown in Fig. S7 in the ESM, the multifilaments consisting of 3, 6, and 10 filaments formed in isopropanol bath showed brighter birefringent textures than their counterparts formed in methanol and ethanol baths, suggesting a more ordered molecular arrangement along the isopropanol-coagulated multifilaments [25]. In addition, the polarized Raman spectrometry was used to evaluate the molecular-level alignment of multifilaments formed in different coagulation baths. All multifilaments exhibited greater normalized intensity in the parallel direction than in the perpendicular direction at the free C=O band of 1731.5 cm^{-1}, exhibiting

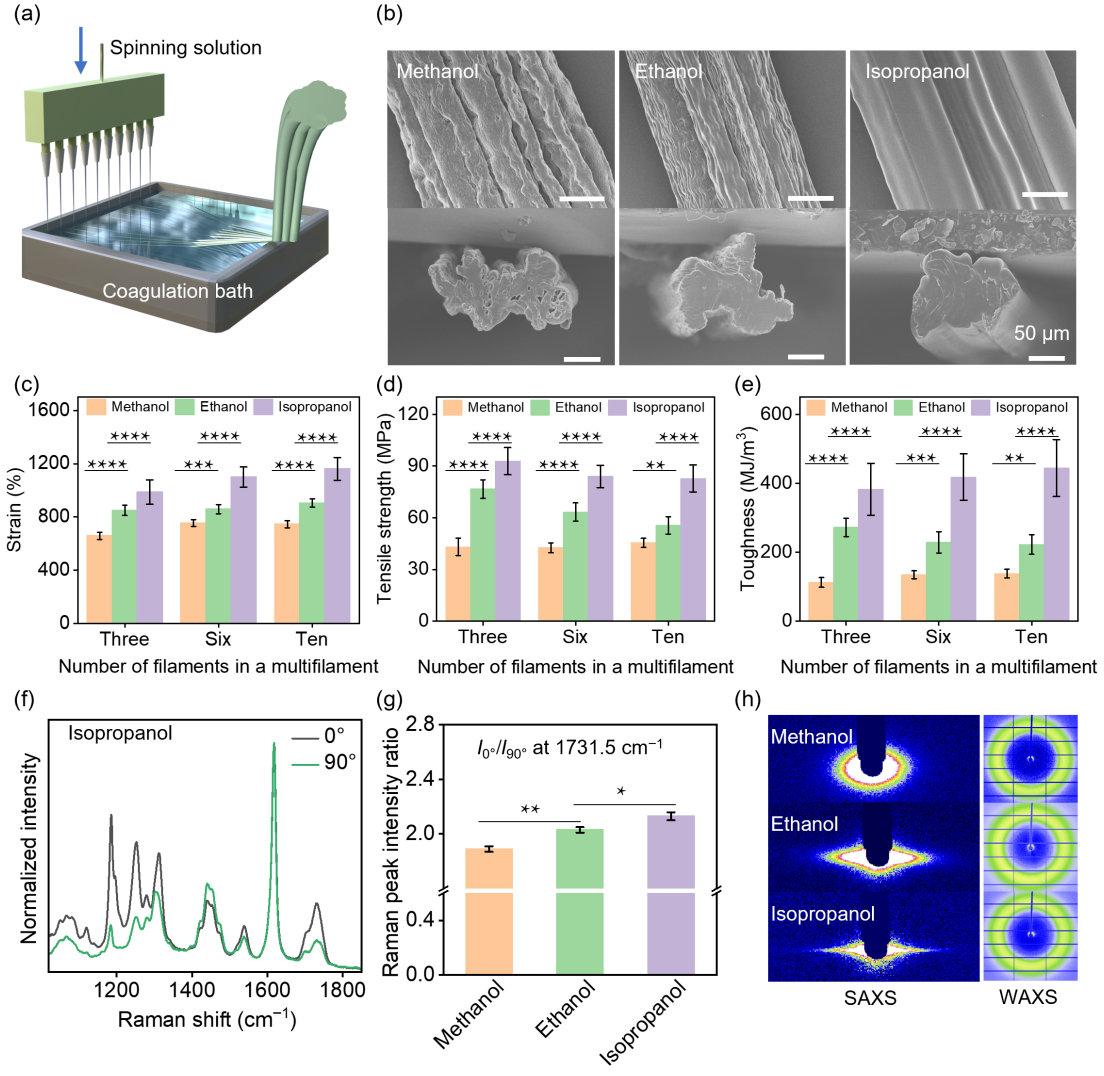

Figure 2 Mechanical performance and characterization of multifilaments consisting of different numbers of filaments formed in different coagulation baths. (a) Schematic illustrating the spinning process of multifilaments. (b) The SEM images of 10-filament multifilaments spun with different coagulation baths. (c) The strain, (d) tensile strength, and (e) toughness analysis of multifilaments consisting of different filament numbers coagulated with different coagulation baths. All data are presented as mean ± standard deviation (SD) (N = 10). The statistical analysis is obtained by the statistical approach of one-way analysis of variance (ANOVA). $^{**}p < 0.01$, $^{***}p < 0.001$, and $^{****}p < 0.0001$. (f) Polarized Raman spectra of multifilaments formed in isopropanol coagulation baths at both parallel (0°) and perpendicular (90°) orientations. (g) The calculated polarized Raman peak intensity ratios of free C=O at 1731.5 cm^{-1} of multifilaments formed in different coagulation baths. All data are presented as mean ± SD (N = 3). The statistical analysis is obtained by the statistical approach of one-way ANOVA. $^{*}p < 0.05$ and $^{**}p < 0.01$. (h) 2D SAXS and corresponding 2D WAXS patterns of 10-filament multifilaments spun with different coagulation baths.

preferential orientation along the parallel direction (Fig. 2(f) and Fig. S8 in the ESM) [26, 27]. Furthermore, the peak intensity ratios of free C=O at 1731.5 cm^{-1} were calculated ($I_{0°}/I_{90°}$) to compare the orientation degree of multifilaments formed in different coagulation baths [8]. As shown in Fig. 2(g), isopropanol-coagulated multifilaments exhibited the highest value, suggesting the most ordered molecular alignment among all multifilaments. The orientation degrees of multifilaments formed in different coagulation baths were further confirmed by two-dimensional (2D) SAXS. The multifilaments showed increasingly sharp streaks as the coagulation bath changed from methanol to ethanol then to isopropanol (Fig. 2(h)), indicating the best orientation degree in isopropanol-coagulated multifilaments [28]. Besides, the crystalline structures of multifilaments were characterized using 2D WAXS. As displayed in Fig. 2(h) and Fig. S9 in the ESM, the multifilaments formed in all coagulation baths showed amorphous structures. In addition, Fourier transform infrared (FTIR) spectroscopy was used to analyse the H-bond in the multifilaments, revealing that the H-bonded C=O content of all samples was approximately 54% [29], with no significant difference (Figs. S10 and S11 in the ESM). These results demonstrated that coagulation bath improved mechanical performance of multifilaments by increasing the degree of orientation and fusion rather than the crystallinity. Better molecular arrangement along the axis and improved fusion were achieved in the multifilaments with decreased polarity of the coagulation bath. According to the "like dissolves like" principle, the polarity difference reflects the compatibility between PU and coagulation bath, which further influences the solvent exchange rate and the formation rate of the multifilaments. Polarity is strongly positively correlated with the solubility parameter, which allows quantitative analysis of the compatibility between PU and the coagulation bath. The solubility parameters of methanol, ethanol, and isopropanol are

29.6, 26.5, and 23.5 $MPa^{1/2}$, respectively [30]. Meanwhile, the hard and soft segments of PU exhibit different solubility parameters, corresponding to 22.78 and 17.0 $MPa^{1/2}$, respectively [31, 32]. Isopropanol, with solubility parameters closest to those of polyurethane, shows the best compatibility and the slowest filament formation rate among alcohols. This resulted in enhanced orientation degree and incompletely solidified filament surface, which promoted the formation of better-fused multifilaments with improved mechanical properties.

3.2 Improve tensile strength of multifilaments via post-stretching

Subsequently, the post-stretching process was applied to the isopropanol-coagulated multifilaments to further enhance their mechanical properties. As shown in Fig. 3(a), the as-spun multifilaments were stretched using two rotating collectors with different rotation speeds. A speed ratio of $v_2 \approx 5v_1$ was selected to balance post-stretching stability with draw ratio. After stretching and heating treatment, the tensile strengths of all multifilaments were significantly improved compared to their as-spun counterparts, reaching 240.78 ± 4.47, 207.99 ± 14.37, and 194.44 ± 3.59 MPa for the post-stretched 3-, 6-, and 10-filament multifilaments, respectively (Fig. 3(b), and Fig. S12 and Table S2 in the ESM). They also displayed high toughness values of 264.10 ± 22.79, 283.69 ± 57.41, 281.52 ± 16.31 MJ/m^3, respectively. The 3-filament multifilaments showed higher tensile strength than 6- and 10-filament ones due to the reduced inter-filament fusion interfaces and gaps in the fewer filaments, resulting in higher tensile strength. Compared to as-spun counterparts, all post-stretched multifilaments showed stable ultimate tensile force with high strains of over 200% (Fig. 3(c)). SEM images showed that the multifilaments became more orderly arranged after the post-stretching treatment, indicating improved molecular alignment in multifilaments (Fig. 3(d), and Figs. S13 and S14 in the ESM). This increased molecular orientation was also revealed by POM, which showed brighter birefringent textures than those observed in the as-spun samples (Fig. 3(e) and Fig. S15 in the ESM). The sharp streaks in 2D SAXS pattern also indicated the well molecular orientation in multifilament upon post-stretching (Fig. 3(f)). Afterwards, the crystallization of post-stretched multifilaments (10-filament) was characterized by WAXS (Fig. 3(g)). In contrast to the amorphous halo observed in as-spun multifilaments, obvious diffraction spots

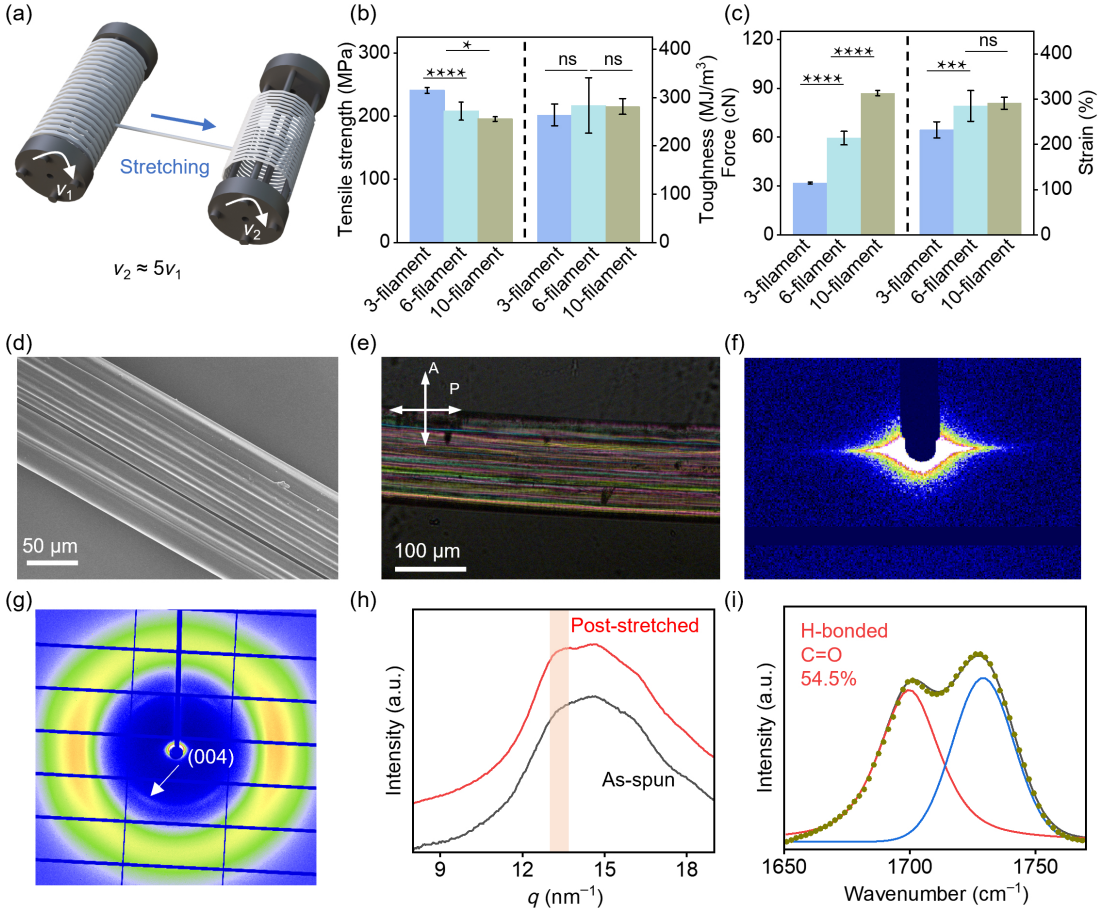

Figure 3 Mechanical performance and characterization of post-stretched isopropanol-coagulated multifilaments. (a) Schematic illustrating the post-stretching of multifilaments conducted with two rotating collectors at different rotation speeds. (b) Tensile strength and toughness analyses of post-stretched multifilaments with different filament counts. (c) Ultimate tensile force and strain analyses of post-stretched multifilaments with different filament counts. (d) SEM image, (e) POM image, (f) 2D SAXS pattern, and (g) 2D WAXS pattern of post-stretched 10-filament multifilaments. (h) 1D WAXS curves along the equator of corresponding 2D WAXS patterns. (i) The deconvolution FTIR peaks in the C=O stretching vibration region of post-stretched 10-filament multifilaments formed in isopropanol bath. The yellow dots, red line, blue line, and black line represent the original data, H-bonded C=O subpeak, free C=O subpeak, and fitted curve, respectively. All statistical data are presented as mean ± SD ($N = 10$). The statistical analysis is obtained by the statistical approach of one-way ANOVA: ns represents no significant difference, $^*p < 0.05$, $^{***}p < 0.001$, and $^{****}p < 0.0001$.

belonging to the (004) plane were observed in 2D WAXS pattern, indicating the formation of crystals. Meanwhile, one-dimensional (1D) WAXS curves along the equator of 2D WAXS patterns showed a gradually increasing peak at about q = 13.0 nm^{-1}, further confirming the existence of crystalline hard domains [33](Fig. 3(h)). The crystallinity was calculated to be 3.60%, resulting from the superposition of the $(\bar{1}01)$ and $(\bar{1}02)$ reflections of crystalline hard segments (Fig. S16 in the ESM). In addition, FTIR revealed that the H-bonded C=O content of post-stretched 10-filament multifilaments was 54.5%, nearly consistent with that in as-spun multifilaments (Fig. 3(i) and Fig. S17 in the ESM). This indicated that post-stretching had no effect on the H-bonded C=O content. Consequently, the post-stretching process increased the tensile strength of multifilaments primarily by improving molecular alignment and crystallization of polyurethane hard domains.

3.3 Scale-up production of spider silk-inspired multifilaments

Based on the above optimized operating parameters, multifilament spinning equipment was set up to produce spider silk-inspired multifilaments on a large scale for practical applications (Fig. 4(a)). This spinning equipment consisted of two coagulation baths, a washing bath, a drying unit, a collector unit, and a series of godet rollers, together with auxiliary devices including a dissolution unit and a controller. To produce multifilaments with more filaments, spinnerets with much more orifices were applied in place of the 3D printing multi-channel microfluidic device (Fig. 4(b)). The obtained multifilaments displayed almost consistent mechanical performances compared to that spun with 3D printing multi-channel microfluidic devices (Figs. S18–S20 in the ESM). The isopropanol-coagulated multifilaments exhibited superior mechanical properties compared to those coagulated in ethanol, demonstrating the scalability of coagulation bath regulation for scale-up multifilament production. However, the slower filaments formation rate in isopropanol coagulation bath led to the incompletely solidified surface as the number of filaments increased, which tended to cause adhesion among filaments on the rotating collectors, thereby hindering continuous production of well-fused multifilaments. Furthermore, the partially solidified surface indicated that the unstable microstructure within filaments was

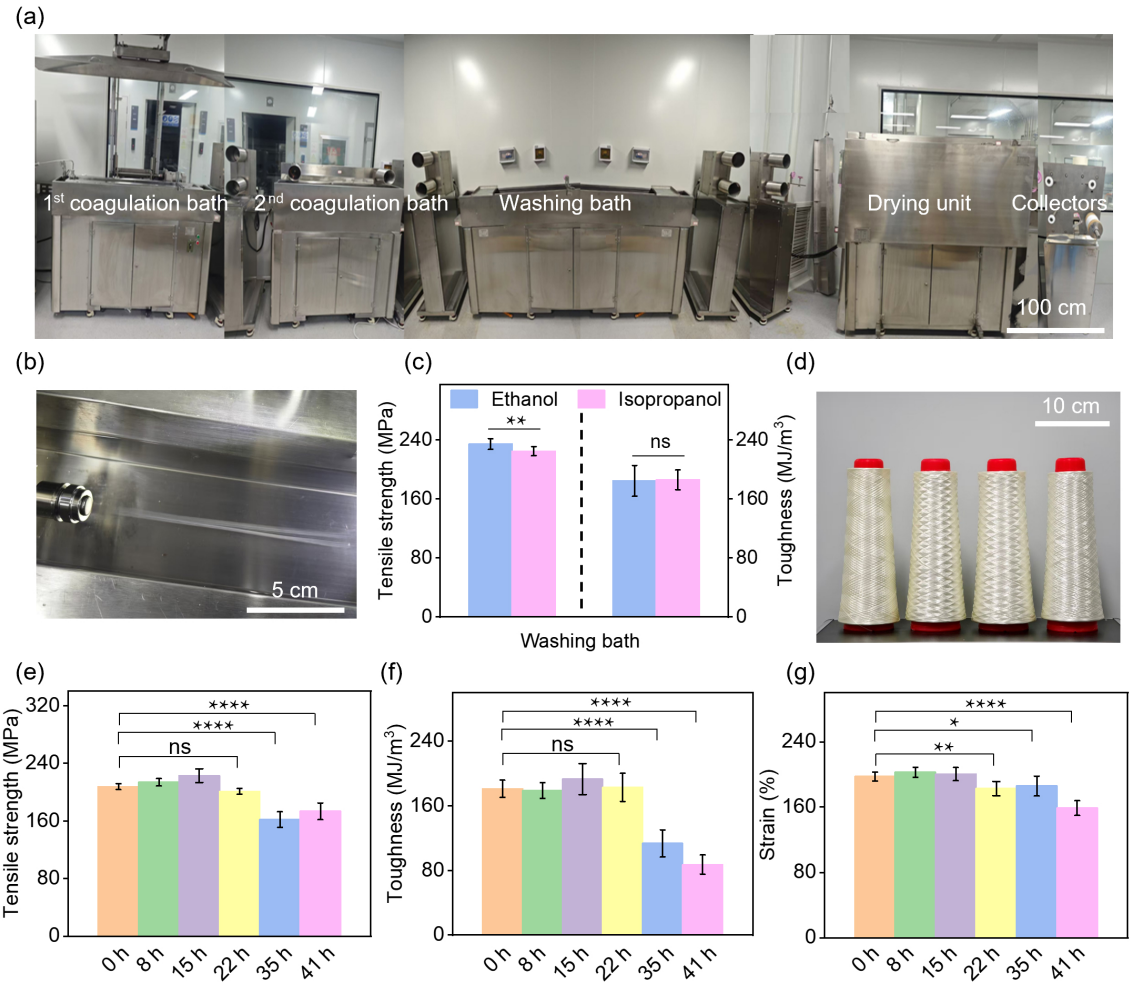

Figure 4 Scale-up production of spider silk-inspired multifilaments. (a) Photograph of designed spinning equipment for large-scale production of spider silk-inspired multifilaments. (b) Photograph of spinning multifilaments using a spinneret. (c) Tensile strength and toughness analyses of multifilaments washed using different washing solvents. The multifilaments washed with ethanol washing bath maintained their original mechanical performance. The data are presented as mean ± SD (N = 10). The statistical analysis is obtained by the statistical approach of t-test: ns represents no significant difference, $^{**}p < 0.01$. (d) Photograph of the large-scale produced multifilaments. (e) Tensile strength, (f) toughness, and (g) strain analyses of multifilaments spun using large-scale spinning equipment that operated for varying durations without changing the coagulation bath. The data are presented as mean ± SD (N = 10). The statistical analysis is obtained by the statistical approach of one-way ANOVA: ns represents no significant difference, $^{*}p < 0.05$, $^{**}p < 0.01$, and $^{****}p < 0.0001$.

susceptible to subsequent ethanol washing bath. To overcome this challenge, a second coagulation bath and a washing bath were added to the entire system. In the second coagulation bath, the multifilaments were looped multiple times around the two rollers at the ends of the bath, ensuring thorough solvent exchange (Fig. S21 in the ESM). This approach prevented the damage of microphase structure in multifilaments during the subsequent washing bath and facilitated the formation of ordered multifilaments with high mechanical properties. After passing through the two coagulation baths, the obtained multifilaments were washed with ethanol in the washing bath to remove excess solvent. Herein, ethanol with a low boiling point was selected as washing solvent, which enabled rapid evaporation in the drying unit, thereby preventing adhesion of the collected multifilaments. The mechanical performance of multifilaments remained unchanged after the washing process, which further validated the rationale for using ethanol as washing solvent (Fig. 4(c), and Figs. S22 and S23 in the ESM). The mechanical properties of the large-scale multifilaments produced in this work were comparable to those of PU fibers reported in literatures at the laboratory scale (Fig. S24 in the ESM) [16, 34–36].

By using this multifilament spinning equipment, continuous production of multifilaments for at least 8 h was achieved. The resulting multifilaments reached a length of approximately 18 km without breaking. (Fig. 4(d)). Notably, the mechanical performances of the multifilaments remained almost unchanged even after a cumulative 22 h of intermittently spinning without changing the coagulation bath (extrusion speed: 0.6 mL/min; and coagulation bath volume: 18 L) (Figs. 4(e)–4(g) and Fig. S25 in the ESM). Upon prolonged operation, excessive DMSO was enriched into the coagulation bath, reaching a concentration of approximately 3.2 vol.%. This elevated DMSO concentration disrupted molecular assembly and filament formation, consequently reducing the mechanical properties of the multifilaments. To extend the duration of continuous production, recirculation systems that control DMSO accumulation by periodically and partially discharging the DMSO/isopropanol mixture and replenishing it with fresh isopropanol can be incorporated.

4 Conclusions

In summary, the large-scale continuous production of spider silk-inspired multifilaments with high strength and toughness was realized using custom-designed spinning equipment. The coagulation bath was modulated to control molecular orientation and interfacial integration of the multifilaments, resulting in enhanced ultimate tensile force, strain, tensile strength, and toughness. In addition, a post-treatment process was employed to further enhance the tensile strength of multifilaments by promoting crystal formation and improving molecular alignment. Furthermore, the second coagulation bath and washing bath were added to ensure a thorough solvent exchange process and continuous spinning. The obtained multifilaments showed a high tensile strength of 234.54 ± 7.37 MPa and a high toughness of 184.68 ± 20.91 MJ/m^3. Moreover, this custom-designed spinning system enabled continuous multifilaments production for more than 8 h, yielding multifilaments exceeding 18 km in length. Notably, even after continuous use of the coagulation bath for approximately one day without replacement, the mechanical properties of multifilaments remained consistent, demonstrating the reliability of the production process. Consequently, through the systematic design and optimization of each process, continuous spinning of spider silk-inspired multifilaments with robust and stable tensile strength and toughness has been achieved, representing a significant step toward the practical application of spider silk-inspired multifilaments.

Electronic Supplementary Material: Supplementary material (methods, SEM images, POM images, FTIR, stress–strain curves, and so on) is available in the online version of this article at https://doi.org/10.26599/NR.2026.94908927.

Data availability

All data needed to support the conclusions in the paper are presented in the manuscript and the Electronic Supplementary Material. Additional data related to this paper may be requested from the corresponding author upon request.

Acknowledgements

This work was supported by the National Natural Science Foundation of China (Nos. T2322025 and 82272161 for J. J. S., Nos. 52402346 and 52572296 for S. K. W., No. 22125701 for K. L., No. 22388101 for H. J. Z., and No. 52472112 for Y. W. L.), the National Key Research and Development Program of China (No. 2024YFA0919300 for K. L.), Beijing Natural Science Foundation (No. QG26006 for S. K. W.), Xiangfu Lab Research Project (No. XF012022C0200 for K. L.), and Jiashan Research Project (No. 2024A41 for S. K. W.). The authors are also thankful for the solid support from the BL19U2 beamline of the National Facility for Protein Science Shanghai (NFPS) and the BL16B1 beamline at SSRF) for assistance during data collection.

Declaration of competing interest

All the contributing authors report no conflict of interests in this work.

Author contribution statement

W. H. C: Data curation, writing manuscript, investigation, visualization. W. W. and L. P. M: Data curation, investigation. Y. W. L, S. K. W., K. L., J. J. S., and H. J. Z.: Project administration, funding acquisition, conceptualization, experimental design, supervision, writing – review & editing. All the authors have approved the final manuscript.

Use of AI statement

None.

References

[1] Rising, A.; Harrington, M. J. Biological materials processing: Time-tested tricks for sustainable fiber fabrication. *Chem. Rev.* **2023**, *123*, 2155–2199.

[2] Miserez, A.; Yu, J.; Mohammadi, P. Protein-based biological materials: Molecular design and artificial production. *Chem. Rev.* **2023**, *123*, 2049–2111.

[3] Omenetto, F. G.; Kaplan, D. L. New opportunities for an ancient material. *Science* **2010**, *329*, 528–531.

[4] Tong, A. X.; Huang, Z. Y.; He, A. N.; Qiao, S. J.; Shi, Z. C.; Wang, X. T.; Chen, Z.; Hu, P. Y.; Wang, K.; Qian, J. et al. A roadmap for extreme-mechanics hydrogels: From toughening mechanisms to intelligent system integration. *Nano-Micro Lett.* **2026**, *18*, 328.
[5] Greco, G.; Mirbaha, H.; Schmuck, B.; Rising, A.; Pugno, N. M. Artificial and natural silk materials have high mechanical property variability regardless of sample size. *Sci. Rep.* **2022**, *12*, 3507.
[6] Xiao, Y.; Yang, Z.; Guo, B. L.; Wu, B. H.; Liu, R. R.; Zhang, S. K.; Zhao, P.; Ruan, J.; Lu, X. Y.; Liu, K. et al. Strong and tough biofibers designed by dual crosslinking for sutures. *Adv. Funct. Mater.* **2024**, *34*, 2313131.
[7] Qin, D. W.; Li, J. J.; Li, H. R.; Zhang, H. J.; Liu, K. Engineered spidroin-derived high-performance fibers for diverse applications. *Nano Res.* **2024**, *17*, 492–502.
[8] Zhang, P.; Jia, B.; Wang, M. Y.; Qin, D. W.; Cheng, W. H.; Wei, Z.; Wan, S. K.; Wang, F.; Li, J. J.; Zhang, H. J. et al. Bagworm silk-mimetic protein fibers with extraordinary stiffness via *in vivo* polymerization and hierarchical self-assembly. *Adv. Funct. Mater.* **2025**, *35*, 2416526.
[9] He, W. Q.; Wang, M. L.; Mei, G. K.; Liu, S. Y.; Khan, A. Q.; Li, C.; Feng, D. Y.; Su, Z. H.; Bao, L. L.; Wang, G. et al. Establishing superfine nanofibrils for robust polyelectrolyte artificial spider silk and powerful artificial muscles. *Nat. Commun.* **2024**, *15*, 3485.
[10] Li, J. H.; Ma, C.; Zhang, H. J.; Liu, K. Engineering mechanical strong biomaterials inspired by structural building blocks in nature. *Chem. Res. Chin. Univ.* **2023**, *39*, 92–106.
[11] Qin, D. W.; Wang, M. Y.; Cheng, W. H.; Chen, J.; Wang, F.; Sun, J.; Ma, C.; Zhang, Y. Y.; Zhang, H. J.; Li, H. R. et al. Spidroin-mimetic engineered protein fibers with high toughness and minimized batch-to-batch variations through β-sheets Co-assembly. *Angew. Chem., Int. Ed.* **2024**, *63*, e202400595.
[12] Wang, M. Y.; Yang, Z. Y.; Jia, B.; Qin, D. W.; Liu, Y. W.; Wang, F.; Sun, J.; Zhang, H. J.; Li, J. J.; Liu, K. Modular protein fibers with outstanding high-strength and acid-resistance performance mediated by copper ion binding and imine networking. *Adv. Mater.* **2024**, *36*, 2400544.
[13] Li, Y. X.; Li, J. J.; Sun, J.; He, H. N.; Li, B.; Ma, C.; Liu, K.; Zhang, H. J. Bioinspired and mechanically strong fibers based on engineered non-spider chimeric proteins. *Angew. Chem., Int. Ed.* **2020**, *59*, 8148–8152.
[14] Blamires, S. J.; Wu, C. C.; Wu, C. L.; Sheu, H. S.; Tso, I. M. Uncovering spider silk nanocrystalline variations that facilitate wind-induced mechanical property changes. *Biomacromolecules* **2013**, *14*, 3484–3490.
[15] Rising, A.; Johansson, J. Toward spinning artificial spider silk. *Nat. Chem. Biol.* **2015**, *11*, 309–315.
[16] Gu, L.; Jiang, Y. Z.; Hu, J. L. Scalable spider-silk-like supertough fibers using a pseudoprotein polymer. *Adv. Mater.* **2019**, *31*, 1904311.
[17] Li, Z. Q.; Zhu, Y. L.; Niu, W. W.; Yang, X.; Jiang, Z. Y.; Lu, Z. Y.; Liu, X. K.; Sun, J. Q. Healable and recyclable elastomers with record-high mechanical robustness, unprecedented crack tolerance, and superhigh elastic restorability. *Adv. Mater.* **2021**, *33*, 2101498.
[18] Wu, S. J.; Liu, Z.; Gong, C. H.; Li, W. J.; Xu, S. J.; Wen, R.; Feng, W.; Qiu, Z. M.; Yan, Y. R. Spider-silk-inspired strong and tough hydrogel fibers with anti-freezing and water retention properties. *Nat. Commun.* **2024**, *15*, 4441.
[19] Wu, R. H.; Bae, J.; Jeon, H.; Kim, T. Spider-inspired regenerated silk fibroin fiber actuator via microfluidic spinning. *Chem. Eng. J.* **2022**, *444*, 136556.
[20] Xiao, Y.; Yang, C. J.; Guo, B. L.; Zhai, X. W.; Lao, S. X.; Zhao, P.; Ruan, J.; Lu, X. Y.; Liu, K.; Chen, D. Bioinspired strong and tough organic-inorganic hybrid fibers. *Small Struct.* **2023**, *4*, 2300080.
[21] Yang, J.; Chen, C. C.; Wang, Y.; Yang, L. J.; Pan, X. L.; Ho, G. W.; Zhang, Q.; Niu, S. C.; Wang, X. Q. Controlled microphase separation and strain programming in hydrogel fibers toward biomimetic architectures and properties. *Nat. Commun.* **2026**, *17*, 17.
[22] Li, M.; Qin, D. W.; Chen, J.; Jia, B.; Wei, Z.; Zhang, Y.; Cheng, W. H.; Liu, Q. Q.; Wang, F.; Li, J. J. et al. Engineered protein fibers with reinforced mechanical properties via β-sheet high-order assembly. *Adv. Sci.* **2024**, *11*, 2410199.
[23] Termonia, Y. Molecular modeling of spider silk elasticity. *Macromolecules* **1994**, *27*, 7378–7381.
[24] Born, L.; Hespe, H.; Crone, J.; Wolf, K. H. The physical crosslinking of polyurethane elastomers studied by X-ray investigation of model urethanes. *Colloid Polym. Sci.* **1982**, *260*, 819–828.
[25] Zhang, Y.; Shi, W. W.; Ma, C.; Wan, S. K.; Li, C.; Shen, J. L.; Li, J. J.; Liu, X. G.; Chen, D.; Wang, F. et al. Superstrong and tough DNA bulk fibers via metal ion-induced multiscale engineering. *Matter* **2024**, *7*, 963–976.
[26] De Santis, A. Photo-polymerisation effects on the carbonyl C=O bands of composite resins measured by micro-Raman spectroscopy. *Polymer* **2005**, *46*, 5001–5004.
[27] Andrikopoulos, K. S.; Chrissanthopoulos, A.; Soto Beobide, A.; Iconomopoulou, S. M.; Moschopoulou, H.; Voyiatzis, G. A. Peculiar behavior of the ester carbonyl vibrational modes in anisotropic aliphatic and semi-aromatic polyesters. *Spectrochim. Acta Part A: Mol. Biomol. Spectrosc.* **2022**, *269*, 120710.
[28] Sun, J.; He, H. N.; Zhao, K. L.; Cheng, W. H.; Li, Y. X.; Zhang, P.; Wan, S. K.; Liu, Y. W.; Wang, M. Y.; Li, M. et al. Protein fibers with self-recoverable mechanical properties via dynamic imine chemistry. *Nat. Commun.* **2023**, *14*, 5348.
[29] Guo, R.; Zhang, Q.; Wu, Y. S.; Chen, H. B.; Liu, Y. H.; Wang, J. J.; Duan, X. L.; Chen, Q.; Ge, Z. S.; Zhang, Y. F. Extremely strong and tough biodegradable poly(urethane) elastomers with unprecedented crack tolerance via hierarchical hydrogen-bonding interactions. *Adv. Mater.* **2023**, *35*, 2212130.
[30] Barton, A. F. M. *CRC Handbook of Solubility Parameters and Other Cohesion Parameters*, 2nd ed.; Routledge: New York, 1991.
[31] Gallu, R.; Méchin, F.; Dalmas, F.; Gérard, J. F.; Perrin, R.; Loup, F. On the use of solubility parameters to investigate phase separation-morphology-mechanical behavior relationships of TPU. *Polymer* **2020**, *207*, 122882.
[32] Ginzburg, V. V.; Bicerano, J.; Christenson, C. P.; Schrock, A. K.; Patashinski, A. Z. Theoretical modeling of the relationship between Young's modulus and formulation variables for segmented polyurethanes. *J. Polym. Sci. Part B: Polym. Phys.* **2007**, *45*, 2123–2135.
[33] Blackwell, J.; Ross, M. X-ray studies of the structure of polyurethane hard segments. *J. Polym. Sci. Polym. Lett. Ed.* **1979**, *17*, 447–451.
[34] Seyedin, S.; Uzun, S.; Levitt, A.; Anasori, B.; Dion, G.; Gogotsi, Y.; Razal, J. M. MXene composite and coaxial fibers with high stretchability and conductivity for wearable strain sensing textiles. *Adv. Funct. Mater.* **2020**, *30*, 1910504.
[35] Gao, X.; Su, J. L.; Xu, C.; Cao, S. C.; Gu, S. J.; Sun, W.; You, Z. W. Water-based continuous fabrication of highly elastic electromagnetic fibers. *ACS Nano* **2024**, *18*, 17913–17923.
[36] Jašo, V.; Milić, J.; Divjaković, V.; Petrović, Z. S. Novel elastomeric polyurethane fibers modified with polypropylene microfibers. *Eur. Polym. J.* **2013**, *49*, 3947–3955.